Spatially single mode photon pair source at 800 nm in periodically poled Rubidium exchanged KTP waveguides

CHRISTOF EIGNER,* ^{ID} LAURA PADBERG, MATTEO SANTANDREA, ^{ID} HARALD HERRMANN, BENJAMIN BRECHT, AND CHRISTINE SILBERHORN ^{ID}

Integrated Quantum Optics, Paderborn University, 33098 Paderborn, Germany
christof.eigner@uni-paderborn.de

Abstract: Photon pair sources in the visible to NIR wavelength region play a key role in quantum optics. The wavelength range around 800 nm provides an opportunity for using low cost detectors, which makes it highly interesting for practical, large scale quantum applications. Here, we report on the realization of single mode Rubidium (Rb) exchanged waveguides in periodically poled (PP) Potassium Titanyl Phosphate (Rb:KTiOPO$_4$ or Rb:KTP) for frequency-non-degenerate type II parametric down-conversion pumped at 400 nm and generating pairs of photons at around 800 nm. The source exhibits a nonlinear conversion efficiency of 2.0%/(Wcm^2), estimated from SHG measurements. Characterisation of the generated two-photon state confirms nonclassical photon-number correlations, characterized by $g^{(1,1)}$. The high nonlinear conversion efficiency and low temperature sensitivity make this source a promising candidate for operations in both classical and quantum integrated network applications.

1. Introduction

Integrated optics plays a key role for efficient nonlinear interactions due to the high confinement over long interaction lengths [1]. To reach high conversion efficiencies, which is necessary for many applications e.g for quantum communication systems, the modal cross section needs to be small, the mode overlap high and the losses low [1]. Nonlinear $\chi^{(2)}$ processes can be tailored to specific interactions by employing quasi-phase matching (QPM) through periodic poling of the material. The ability to produce poling periods in the range between 1-100 µm allows for the realization of a wide variety of processes involving wavelengths spanning a broad range. Combining electric field poling and waveguide fabrication methods, QPM waveguide devices have become of interest in several applications like spectroscopy, metrology, sensing and quantum optics [2,3].

Several attempts have been made to realize integrated photon pair sources in the 800 nm wavelength regime. This wavelength regime is a promising candidate for a large quantum network, as it coincides with the operating region of many quantum memories and low-cost, high-efficiency detectors are readily available. Producing these photon pairs generally requires pumping at UV wavelengths, where absorption and photorefraction typically limit device performance. The material properties of Potassium Titanyl Phosphate (KTiOPO$_4$; short KTP) make it an ideal candidate for applications in the visible to near infrared wavelength regime, due to its high resistance to photorefraction, broad transparency in the UV range and insensitivity to changes in operating temperature.

Several groups have begun developing KTP waveguide sources producing photon pairs at around 800 nm, however, these devices are spatially multi mode at this wavelength regime [4–8]. Due to mixing between different spatial modes, these multi mode waveguides are often incapable of producing photon pairs in a single output mode. Although spectral filtering can sometimes

be used to address this problem, in many cases this is not possible due to the overlap between them [6,7]. This limits the suitability of these sources for use within large quantum networks. In contrast, single mode waveguides at the parametric down-conversion (PDC) wavelengths are capable of producing photon pairs in a single output mode. This significantly reduces the requirements for spectral filtering and also increases the process brightness because a portion of the pump power is no longer lost to pumping undesired output modes. Spatially single mode operation at 800 nm has been shown, e.g. in femtosecond laser written [9] and Rb-exchanged ridge waveguides [10] designed for second harmonic generation (SHG) from 800 nm to 400 nm.

Here we report on the fabrication and characterisation of a spatially single mode KTP waveguide demonstrating single mode photon pair generation at 800 nm. The device is fabricated using electric field periodic poling to produce the desired QPM grating and Potassium-Rubidium exchange to define the guiding region. Classical (SHG) and quantum (PDC) characterisation of the device is performed, with the results highlighting the suitability of the presented platform for the generation of single mode photon pairs at 800 nm.

2. Sample fabrication

We fabricated near-surface Rb-exchanged waveguides in periodically poled KTP samples with dimensions of 11-6-1 mm^3 along the crystallographic a, b and c axes, cut from a commercially available flux-grown wafer. An overview of the process is given in Fig. 1(a-c). First, the samples were periodically poled with periods from 8.1 μm to 8.6 μm, by patterning the -c face of the KTP crystal with a periodic structure of insulating photo resist and a subsequent electric-field poling. Both sides (+c and -c) were coated with a metallic layer to provide electrical contact, which we used to apply four high voltage pulses of 2.7 kV to invert the spontaneous polarization. The pulses had a trapezoidal shape with 1 ms rising and falling time and a 2 ms plateau, at which the domain inversion takes place. To monitor the poling progress, we used an in-situ non-destructive monitoring technique (as developed by Karlsson et al. [11,12]), based on the electro-optically induced differential phase retardation of a laser beam. For waveguide fabrication we had to remove the metal electrodes in an ammonia solution, which acts as a weak selective etchant for the domain orientation, too. All samples were etched to a depth of about 5 nm to visualize the domain structure, see Fig. 1(c). By increasing the etching time and temperature, topographic patterns up to 100 nm can potentially be achieved. The drawback of this method is an increased roughness of the surface which also increases the waveguide losses. A better, non-destructive method to visualize the domain structure is confocal Raman spectroscopy [13], which allows for domain investigation also in the depth of the crystal.
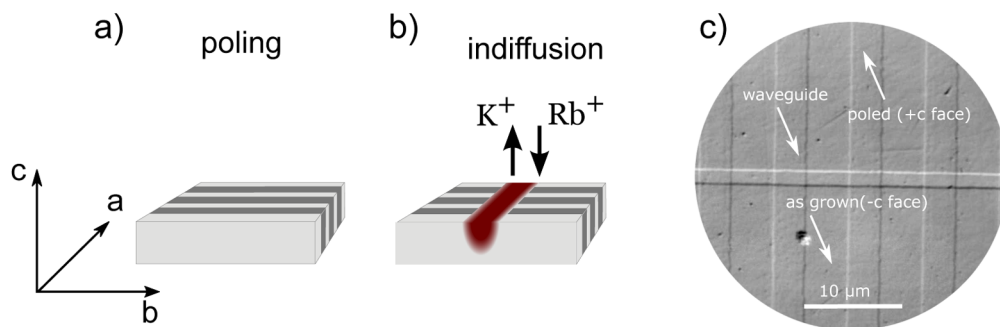

Fig. 1. (a) We first periodically pole the KTP sample in which we (b) fabricated waveguides along the a-axis by a subsequent Rb-exchange in a masked Rb-K ion exchange. In the (c), a selectively etched c-surface is shown. In the centre part the waveguide is shown in horizontal direction along the a-axis of the crystal.

Next, we fabricated waveguides along the a-axis in the periodically poled substrates on the former -c face of the crystal. To locally increase the refractive index and thus create a guiding structure, we exchanged Potassium in the crystal against Rubidium. For this ion exchange, we used a melt with a composition of 97 mol% $RbNO_3$, 1 mol% $Ba(NO_3)_2$ and 2 mol% KNO_3 at a temperature of 330 °C for 5 min. These parameters allow for the fabrication of single mode waveguides at 800 nm with a symmetric spatial mode profile. The exchange depth of the Rb ions is controlled by the melt composition, the exchange temperate and exchange time. Using energy-dispersive X-ray spectroscopy (EDX) we found that the exchange depth of a 2.5 µm waveguide was (8±0.4) µm. The lateral control of the exchange is done by a Titanium mask. We fabricated slits in the Titanium layer by photolithographic patterning and a subsequent wet etching of the Titanium to form an exchange mask. The slit widths vary from 1.5 µm to 4.5 µm with 0.5 µm spacing. After preparing the waveguides, the end facets were polished in a physical chemical polishing process to prepare for light coupling.

3. Waveguide properties

To test the performance of our structures, we first studied the linear optical properties of the waveguides. All waveguides with width from 1.5 to 4.5 µm guide light in a single mode at the fundamental wavelength of 800 nm. We measured the near field of the fundamental modes at 800 nm (see Fig. 2). The mode diameter in the x-direction shows the expected growth in diameter with increasing waveguide width. However, the y-direction shows a growing mode diameter with decreasing waveguide width. We attribute this behavior to an increasing diffusion depth in narrower waveguides. This effect is outside the scope of this paper but has been investigated in a different publication [14]. For an efficient coupling into the waveguide, a good overlap with a Gaussian mode is required. We achieved a symmetric mode profile for both polarizations in 3 µm wide waveguides (see Fig. 3). The fabricated waveguides have a graded-index profile in the depth direction. In order to compare with experimental results in the following, simulations were performed assuming an error-function shaped index profile as used in [15]. For mode overlap
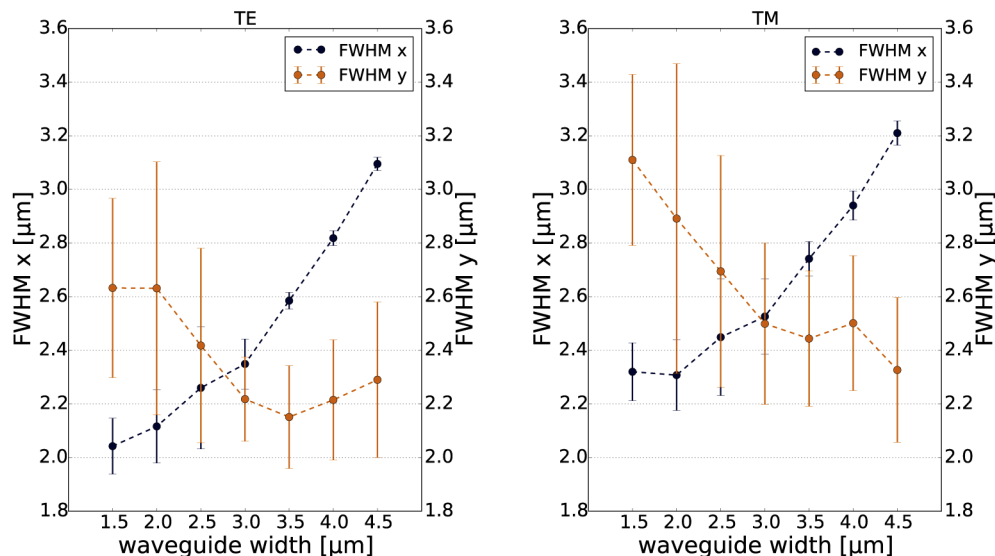

Fig. 2. Measurements of the FWHM in lateral and vertical direction for TE and TM polarization depending on the waveguide width. The FWHM of several (>4) waveguides were measured in order to retrieve the shown measurement uncertainties.

calculations we reproduced the modes using a finite element method program (FEMSim tool from RSoft) to calculate the refractive index increase at the surface of the waveguide Δn_0 for both polarizations. The waveguide widths were defined by the mask and their depth was measured with EDX, leaving Δn_0 as the only fitting parameter between the simulated and the experimental data. For the refractive index increase at the surface we thereby estimated $\Delta n_{0,\,\text{TE}} = 0.01 \pm 0.005$ for TE and $\Delta n_{0,\,\text{TM}} = 0.011 \pm 0.005$ for TM polarization. The field overlap between the calculated and measured mode was above 0.96 for both modes, indicating a good fit.
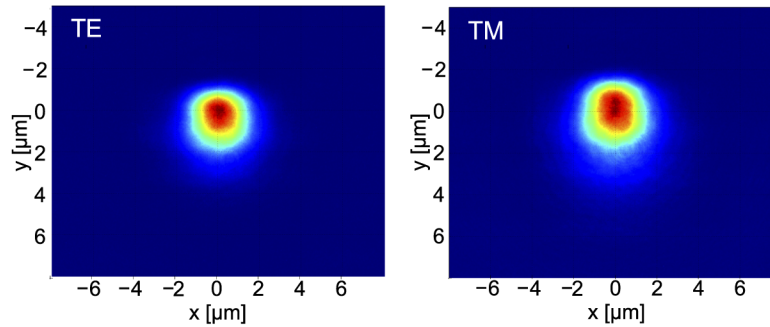

Fig. 3. Measured near-field distribution of the fundamental mode at 800 nm in both polarizations. The waveguide with a dimension 3 µm width and 8 µm depth, only one mode is guided in both polarizations exhibit a symmetric mode profile.

Afterwards, we measured the losses of the waveguides at a wavelength of 888 nm, using the Fabry-Perot method [16]. We scanned the optical path length of the resonator by varying the sample temperature between 20°C and 60°C. From the contrast of the Fabry-Perot oscillations, we calculated the transmission losses of our waveguides. We could achieve attenuation coefficients of 1.3±0.2 dB/cm (1.8±0.2 dB/cm) for TM (TE) polarization in 10 mm-long samples (see Fig. 4). These propagation losses are comparable to losses obtained for samples at 1550 nm of 0.85 dB/cm and 0.67 dB/cm for TE and TM polarizations, respectively [3].
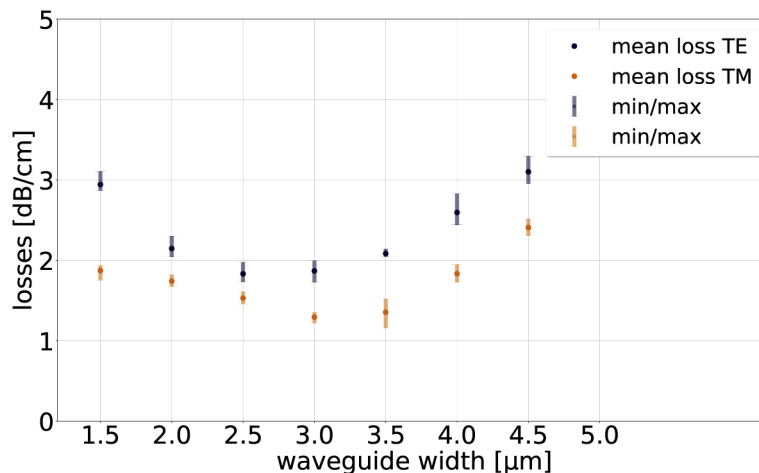

Fig. 4. Loss measurements in channel waveguides for different waveguide widths. The dots indicate the mean value for the losses, the error bar corresponds to the minimum and maximum value of the measured losses for each waveguide width.

4. Second harmonic generation

In the next step we measured the generated second harmonic light in a waveguide with poling period of 8.64 μm in a type-II quasi-phase matched process designed for 800 nm to 400 nm conversion. Linearly polarised light from a cw Ti:Sapphire laser (M2 SolsTis) at 800 nm with a rotation of 45° with respect to the crystallographic c-axis is coupled to the channel waveguide via lens coupling (see Fig. 5(a)). Power and polarization are controlled with a half-wave plate, a polarising beam splitter and an additional half-wave plate. In the waveguide, horizontally polarised light is generated in a type-II phase matched process at half the pump wavelength. After the waveguide, we used a short-pass and a colour glass filter to suppress the pump light. We measured the generated second harmonic (SH) power as a function of the pump wavelength with a photo diode as shown in the inset of Fig. 6(a). For the main peak the measurements confirm the expected sinc-function, with superimposed Fabry-Perot type oscillations. Our data also show a broad plateau ranging over a range of 2 nm. We attribute this plateau and deviations from the envelope sinc function to inhomogeneities in the poling and the waveguide itself [17,18]. From fitting a sinc function to the dominant phase matching peak, we obtain an effective interaction length $l_{effective}$ of 10 mm (Fig. 6(a), red solid line). The deviation from the expected peak for the actual poling length of 14 mm (Fig. 6(a), green dashed line) originates most likely from an inhomogeneous poling. The SHG efficiency is calculated as

$$\eta_{exp} = \frac{P_{SHG}}{P_{Pump}^2 \cdot l^2} \cdot 100\% = 2.0 \frac{\%}{W \cdot cm^2}, \tag{1}$$

where P_{SHG} is the measured SH power, P_{pump} is the pump power and l is the length of the poled fraction of the crystal. We measured these values in a 2.5 μm wide waveguide of length $l_{poled} =$ 14 mm, a poling period of Λ=8.64 μm, a pump wavelength of 801.3 nm and a pump power of 195 mW in front of the waveguide, resulting in a second harmonic power of 50 μW. We corrected
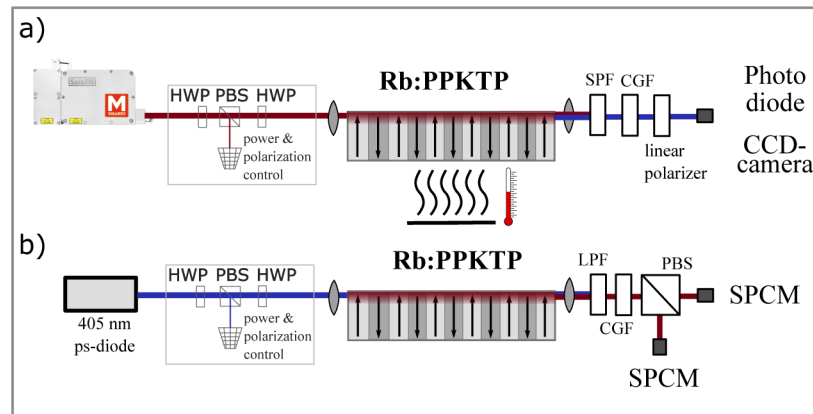

Fig. 5. Optical setups to investigate the optical properties of the device. We show the SHG characterisation setup in a). Power and polarization are controlled by a combination of a half wave plate (HWP), a polarising beam splitter (PBS) and an additional HWP. The light is coupled into the waveguide with an 8mm lens. The generated light is collimated with another lens, which is AR coated for 400nm. The pump light is filtered with a short pass filter (SPF) and an additional colour glass filter (CGF). The linear polarizer allows for an analysis of the SH light polarization. In b), we show the setup for PDC experiments. The incoupling lens is AR coated for 400 nm, while the outcoupling lens is AR coated for 700 nm-1000 nm. And additional PBS is used to split the orthogonally polarised PDC photons. The photons are detected on single photon counting modules (SPCM).

them for end facet reflection losses (Fresnel reflection of T=0.91 for pump wavelength and T=0.89 for SH wavelength) and transmission losses of the two coloured-glass filters (2 x T=0.80) at the SH wavelength, resulting in a corrected pump power of 176.5 mW and a corrected SH power of 88 μW. We finally estimated the efficiency to be $\eta_{exp} = 2.0\%/(Wcm^2)$. A comparison of normalized efficiency with previous demonstrations of SHG in PPKTP waveguides is shown in Table 1.
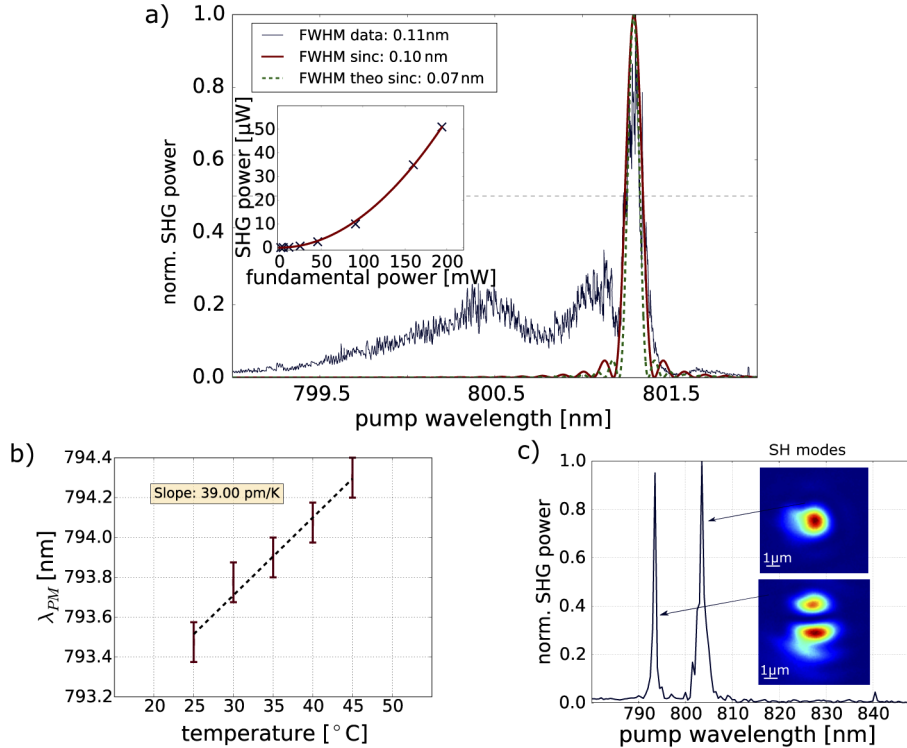

Fig. 6. a) Measured (blue) and calculated (red) phase matching curve of a 2.5 μm wide and an effectively 10 mm long channel waveguide for type-II conversion; the calculated curve (green) corresponds to the sample length of 14 mm. The inset shows the Input-Output curve of fundamental to second harmonic power. b) Temperature dependence of the phase matching wavelength. c) SHG spectra for different modes and their near field image.

Table 1. Comparison of efficiency for periodically poled bulk or waveguides in KTP.

	material	type	pump	second harmonic wavelength [nm]	efficiency
1	this work	II	cw	400.6	$2.0\,\%/(W\cdot cm^2)$
2	ridge waveguide [10]	II	cw	396.1	$6.6\,\%/(W\cdot cm^2)$
3	laser written waveguide [19]	II	cw	471	$4.6\,\%/(W\cdot cm^2)$
4	segmented waveguide [20]	II	cw	508	$10\,\%/(W\cdot cm^2)$
5	Rb diffused waveguide [21]	II	pulsed	398.3	$4.78\,\%/(W\cdot cm^2)$
6	bulk KTP [22]	II	pulsed	398	$1.79\,\%/(W\cdot cm)$
7	segmented waveguide [23]	I	cw	425	$127\,\%/(W\cdot cm^2)$
8	segmented waveguide [20]	I	cw	394	$84\,\%/(W\cdot cm^2)$

We also determined the theoretically expected efficiency. Therefore, we calculated the mode overlap integral S by integrating the scalar amplitude of the electric field distributions of the two pump fields ($E_{pump-TE}$, $E_{pump-TM}$) and the SH field (E_{SH-TE}). We obtained these values by modelling the modes in RSoft using the same refractive index increase for fundamental and second harmonic mode. The obtained value of the overlap integral is $S = 0.25 m^{-1}$ and was used to calculate a theoretically expected efficiency of

$$\eta_{theo} = \frac{8\pi^2 d_{QPM}^2 S^2}{n^3 c \epsilon_0 \lambda_{pump}^2} = 6.8 \frac{\%}{W \cdot cm^2}. \qquad (2)$$

Here c is the speed of light, n = 1.84 is the refractive index of the SH wave [24], λ_{pump} is the pump wavelength, S is the overlap integral of the three fields and $d_{QPM} = 2/\pi \cdot d_{24} = 2/\pi \cdot 1.9$ pm/V [25]. The reduction of the experimental efficiency with respect to the theory is caused mainly by waveguide losses, which are particularly high for the SH modes, and by inhomogeneities in the grating structure.

Finally, we measured the temperature dependence of the phase matching to be 39 pm/K in a range from 25°C to 45°C (see Fig. 6(b)), which is in good agreement with temperature dependent phase matching measurements in PPKTP bulk crystals (60 pm/K) [26]. The device showed temperature insensitive behavior which allows stable operation, independent of the ambient conditions.

5. Parametric down conversion

The photon-pair generation from type II PDC of the source was then investigated. To pump the waveguide, we used a picosecond pulsed laser diode (Picoquant LDH-P-C-400B) at 405 nm. The laser has a spectrum of 2 nm, a pulse duration of 50 ps, a repetition rate of 1MHz and was coupled to a single mode fibre to symmetrize the mode shape. The light is coupled into the waveguide with a lens of focal length f=4.5 mm, which allows for mode shaping in order to selectively excite different modes. The uncorrected power of the transmitted light was found to be 2.9 µW. At the output of the sample, the pump light is blocked by a combination of a colour glass filter and a long-pass filter, while the PDC photons are seperated using a polarising beam splitter. They are detected either with a single-photon sensitive spectrometer (Andor iKon-M SR-303i-A), or with single photon counting modules (PerkinElmer SPCM-AQR-13FC). Though the waveguide is single mode at 800 nm, it still guides several modes at the pump wavelength of 405 nm. Figure 7 shows the measured PDC spectra for different spatial pump modes indicated by the insets. The spectrum is not corrected for detection efficiency of the spectrometer, which reduces the number of counts at longer wavelengths. A detailed analysis of the phase matching properties of PDC sources which are multi mode at the pump wavelength can be found in [27].

Owing to the single mode design at 800nm, the generated PDC photons are in the fundamental waveguide mode, which significantly reduces the number of spectral peaks in comparison to multi mode waveguides, by eliminating the overlap between neighboring phase matching contributions [7,28]. The lower number and wider separation of spectral modes decreases the required amount of filtering and also increases the process brightness, because a portion of the pump power is no longer lost to pumping undesired output modes. Further, the output alignment to fibers can be realized with less effort compared to existing multi mode sources.

To further characterize the performance of our PDC source, we measured the Klyshko efficiency [29]. This number measures the probability of detecting a signal (idler) photon upon a herald detection of an idler (signal) and hence provides a measure of the overall efficiency of the setup
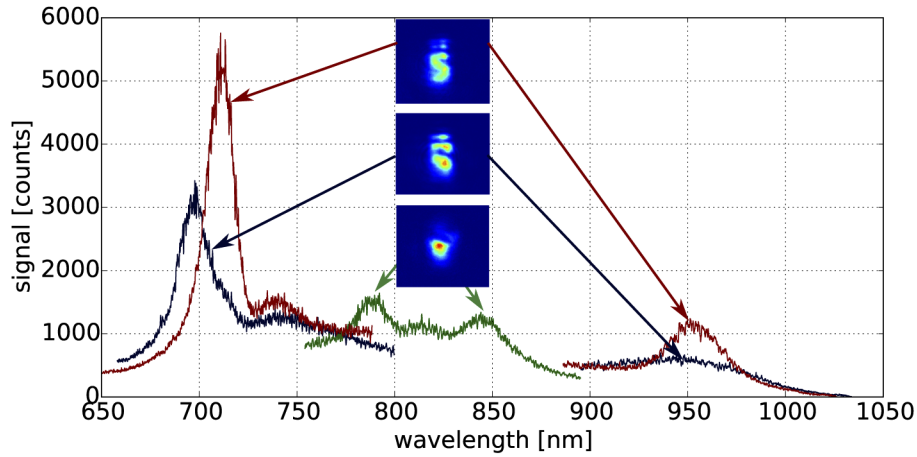
Fig. 7. Measured PDC spectra for different pump mode combinations. The spatial mode images for the 405 nm mode are shown in the insets.

including all losses and detection efficiencies. The Klyshko efficiency [30] is given by

$$
\begin{aligned}
\eta_{\text{signal}} &= \frac{\text{coincidence rate}}{\text{idler rate}} \\
\eta_{\text{idler}} &= \frac{\text{coincidence rate}}{\text{signal rate}}
\end{aligned}
\tag{3}
$$

From the output of the single photon detectors, at a wavelength of 720 nm for the signal photons and 950 nm for the idler photons, we calculated the Klyshko efficiencies to be 8.6% and 7.2% for signal and idler, respectively. We estimated the maximum achievable Klyshko to be 16% and 9% for signal and idler, respectively, by taking into account the detector efficiencies (($\eta_{\text{Det signal}}$=65% and $\eta_{\text{Det idler}}$=25%)) and the optical transmission of the setup (T_{signal} = 0.26 and T_{idler} = 0.38). The Klyshko efficiency of the idler photon is close to the expected value, supporting the previously measured waveguide loss, transmission efficiency and waveguide to fiber coupling are correct. It is believed that the lower than expected Klyshko efficiency in the signal arm is either due to additional losses in one fiber connector that could not be characterized or due to increased waveguide losses at the signal wavelength. The measured Klyshko efficiencies are comparable to values measured in multi mode waveguides (9% [7] and 16.5% [31]), where a much larger amount of filtering was necessary in order to reduce the background and filter down to a single spatial mode. The Klyshko efficiency can be improved by using optimized filters with lower transmission losses.

Finally, we investigated the nonclassicality of the output of our PDC source by means of normalised Glauber correlation functions [32]. For any two-mode field exhibiting classical correlations, the following Cauchy-Schwarz inequality must hold:

$$
\left| g_{s,i}^{(1,1)} \right| \leq \sqrt{g_s^{(2)} g_i^{(2)}}, \tag{4}
$$

where $g_{s,i}^{(1,1)} = \langle \hat{a}_s^\dagger \hat{a}_s \hat{b}_i^\dagger \hat{b}_i \rangle / (\langle \hat{a}_s^\dagger \hat{a}_s \rangle \langle \hat{b}_i^\dagger \hat{b}_i \rangle)$ is the normalised broadband signal-idler cross-correlation function and $g_s^{(2)} = \langle \hat{a}_s^\dagger \hat{a}_s^\dagger \hat{a}_s \hat{a}_s \rangle / \langle \hat{a}_s^\dagger \hat{a}_s \rangle^2$ is the normalised broadband signal autocorrelation function (and similar for $g_i^{(2)}$) [33]. The cross correlation function $g^{(1,1)}$ denotes the probability for measuring a signal-idler coincidence click (1 click in signal, 1 click in idler) normalised to the product of the signal and idler click probabilities and is as such a second-order correlation. In

addition, note that our experiment is operating in a regime where the duration of the generated quantum state is much longer than the detection time window (~ps vs ~ns), such that the time dependence of the Glauber correlation functions averages out. For an ideal single-mode PDC, the marginal photon number statistics are thermal, hence $g_s^{(2)} = g_i^{(2)} = 2$, and, using Eq. (4), we obtain a classical limit of

$$\left| g_{s,i}^{(1,1)} \right| \leq 2. \tag{5}$$

The g(1,1) function can be calculated from our measured detector clicks as

$$g_{s,i}^{(1,1)} = \frac{N_c}{N_s \cdot N_i} \cdot N_{te}, \tag{6}$$

where N_c is the number of coincidence clicks, N_s the signal and N_i the idler clicks, N_{te} are the trigger events. For a typical measurement at wavelengths of 720 nm (950 nm) for the signal (idler) photons and an integration time of 1 s, we find

$$g_{s,i}^{(1,1)} = \frac{151}{2429 \cdot 1932} \cdot 1 \cdot 10^6 = 32 \pm 4 \geq 2, \tag{7}$$

clearly exceeding the classical limit of 2. Errors were calculated by assuming Poissonian errors for the recorded click numbers. This confirms that our PDC source generates high-quality nonclassically correlated photon pairs with a significance of more than seven standard deviations.

6. Conclusion

In this work, we fabricated spatially single-mode, periodically poled Rb:KTP waveguides for 800 nm and used them to demonstrate photon-pair generation via PDC. The device shows relatively low transmission losses and symmetric mode profiles. Furthermore, we successfully demonstrated type-II second harmonic generation from 801.2 nm to 400.6 nm with normalized conversion efficiency of 2.0%/(Wcm^2), phase matching bandwidth of 0.1 nm and a temperature dependence of 39 pm/K. The demonstration of an integrated device producing single photon pairs in a single spatial mode with high conversion efficiency and low temperature dependence shows that our source is an excellent candidate for the generation of PDC states in the visible spectrum.

Disclosures

The authors declare no conflicts of interest.

References

1. T. Suhara and M. Fujimura, *Waveguide Nonlinear-Optic Devices* (Springer Berlin Heidelberg, 2003).
2. Y. Yu, F. Ma, X.-Y. Luo, B. Jing, P.-F. Sun, R.-Z. Fang, C.-W. Yang, H. Liu, M.-Y. Zheng, X.-P. Xie, W.-J. Zhang, L.-X. You, Z. Wang, T.-Y. Chen, Q. Zhang, X.-H. Bao, and J.-W. Pan, "Entanglement of two quantum memories via fibres over dozens of kilometres," Nature **578**(7794), 240–245 (2020).
3. V. Ansari, E. Roccia, M. Santandrea, M. Doostdar, C. Eigner, L. Padberg, I. Gianani, M. Sbroscia, J. M. Donohue, L. Mancino, M. Barbieri, and C. Silberhorn, "Heralded generation of high-purity ultrashort single photons in programmable temporal shapes," Opt. Express **26**(3), 2764–2774 (2018).

4. M. Karpiński, C. Radzewicz, and K. Banaszek, "Experimental characterization of three-wave mixing in a multimode nonlinear KTiOPO$_4$ waveguide," Appl. Phys. Lett. **94**(18), 181105 (2009).

5. A. Christ, K. Laiho, A. Eckstein, T. Lauckner, P. J. Mosley, and C. Silberhorn, "Spatial modes in waveguided parametric down-conversion," Phys. Rev. A **80**(3), 033829 (2009).

6. P. J. Mosley, A. Christ, A. Eckstein, and C. Silberhorn, "Direct measurement of the spatial-spectral structure of waveguided parametric down-conversion," Phys. Rev. Lett. **103**(23), 233901 (2009).

7. K. Laiho, K. N. Cassemiro, and C. Silberhorn, "Producing high fidelity single photons with optimal brightness via waveguided parametric down-conversion," Opt. Express **17**(25), 22823–22837 (2009).

8. M. Karpiński, C. Radzewicz, and K. Banaszek, "Nonlinear waveguide source of entangled photon pairs in single spatial modes," *Frontiers in Optics 2011/Laser Science XXVII* (OSA, 2011).

9. F. Laurell, T. Calmano, S. Müller, P. Zeil, C. Canalias, and G. Huber, "Laser-written waveguides in KTP for broadband Type II second harmonic generation," Opt. Express **20**(20), 22308–22313 (2012).

10. C. Eigner, M. Santandrea, L. Padberg, M. F. Volk, C. E. Rüter, H. Herrmann, D. Kip, and C. Silberhorn, "Periodically poled ridge waveguides in KTP for second harmonic generation in the UV regime," Opt. Express **26**(22), 28827–28833 (2018).

11. H. Karlsson and F. Laurell, "Electric field poling of flux grown KTiOPO4," Appl. Phys. Lett. **71**(24), 3474–3476 (1997).

12. H. Karlsson, F. Laurell, and L. K. Cheng, "Periodic poling of RbTiOPO4 for quasi-phase matched blue light generation," Appl. Phys. Lett. **74**(11), 1519–1521 (1999).

13. M. Rüsing, C. Eigner, P. Mackwitz, G. Berth, C. Silberhorn, and A. Zrenner, "Identification of ferroelectric domain structure sensitive phonon modes in potassium titanyl phosphate: A fundamental study," J. Appl. Phys. **119**(4), 044103 (2016).

14. L. Padberg, M. Santandrea, M. Rüsing, J. Brockmeier, P. Mackwitz, G. Berth, A. Zrenner, C. Eigner, and C. Silberhorn, "Characterisation of width-dependent diffusion dynamics in rubidium-exchanged KTP waveguides," Opt. Express **28**(17), 24353 (2020).

15. M. F. Volk, C. E. Rüter, M. Santandrea, C. Eigner, L. Padberg, H. Herrmann, C. Silberhorn, and D. Kip, "Fabrication of low-loss Rb-exchanged ridge waveguides in z-cut KTiOPO4," Opt. Mater. Express **8**(1), 82–87 (2018).

16. R. Regener and W. Sohler, "Loss in low-finesse Ti:LiNbO3 optical waveguide resonators," Appl. Phys. B **36**(3), 143–147 (1985).

17. M. Santandrea, M. Stefszky, and C. Silberhorn, "General framework for the analysis of imperfections in nonlinear systems," Opt. Lett. **44**(22), 5398–5401 (2019).

18. M. Santandrea, M. Stefszky, G. Roeland, and C. Silberhorn, "Characterisation of fabrication inhomogeneities in Ti:LiNbO3 waveguides," New J. Phys. **21**(12), 123005 (2019).

19. S. Müller, T. Calmano, P. W. Metz, C. Kränkel, C. Canalias, C. Liljestrand, F. Laurell, and G. Huber, "Highly efficient continuous wave blue second-harmonic generation in fs-laser written periodically poled Rb:KTiOPO4 waveguides," Opt. Lett. **39**(5), 1274–1277 (2014).

20. F. Laurell, J. B. Brown, and J. D. Bierlein, "Simultaneous generation of UV and visible light in segmented KTP waveguides," Appl. Phys. Lett. **62**(16), 1872–1874 (1993).

21. R. Machulka, J. Svozilík, J. Soubusta, J. Peřina, and O. Haderka, "Spatial and spectral properties of fields generated by pulsed second-harmonic generation in a periodically poled potassium-titanyl-phosphate waveguide," Phys. Rev. A **87**(1), 013836 (2013).

22. A. Zukauskas, V. Pasiskevicius, and C. Canalias, "Second-harmonic generation in periodically poled bulk Rb-doped KTiOPO4 below 400 nm at high peak-intensities," Opt. Express **21**(2), 1395 (2013).

23. W. P. Risk, W. J. Kozlovsky, S. D. Lau, G. L. Bona, H. Jaeckel, and D. J. Webb, "Generation of 425-nm light by waveguide frequency doubling of a GaAlAs laser diode in an extended-cavity configuration," Appl. Phys. Lett. **63**(23), 3134–3136 (1993).

24. K. Kato, "Temperature insensitive SHG at 0.5321 µm in KTP," IEEE J. Quantum Electron. **28**(10), 1974–1976 (1992).

25. I. Shoji, T. Kondo, A. Kitamoto, M. Shirane, and R. Ito, "Absolute scale of second-order nonlinear-optical coefficients," J. Opt. Soc. Am. B **14**(9), 2268 (1997).

26. A. Arie, G. Rosenman, V. Mahal, A. Skliar, M. Oron, M. Katz, and D. Eger, "Green and ultraviolet quasi-phase-matched second harmonic generation in bulk periodically-poled KTiOPO4," Opt. Commun. **142**(4-6), 265–268 (1997).

27. M. Jachura, M. Karpiński, K. Banaszek, D. Bharadwaj, J. Lugani, and K. Thyagarajan, "Generation and characterization of discrete spatial entanglement in multimode nonlinear waveguides," Phys. Rev. A **95**(3), 032322 (2017).

28. A. Eckstein, A. Christ, P. J. Mosley, and C. Silberhorn, "Highly efficient single-pass source of pulsed single-mode twin beams of light," Phys. Rev. Lett. **106**(1), 013603 (2011).

29. D. N. Klyshko, "Use of two-photon light for absolute calibration of photoelectric detectors," Sov. J. Quantum Electron. **10**(9), 1112–1117 (1980).

30. B. Zel'Dovich and D. Klyshko, "Field statistics in parametric luminescence," JETPL **9**, 40 (1969).

31. K. Laiho, K. N. Cassemiro, D. Gross, and C. Silberhorn, "Probing the negative wigner function of a pulsed single photon point by point," Phys. Rev. Lett. **105**(25), 253603 (2010).

32. R. J. Glauber, "Coherent and incoherent states of the radiation field," Phys. Rev. **131**(6), 2766–2788 (1963).

33. A. Christ, K. Laiho, A. Eckstein, K. N. Cassemiro, and C. Silberhorn, "Probing multimode squeezing with correlation functions," New J. Phys. **13**(3), 033027 (2011).